Impact of a Lifshitz transition on the onset of spontaneous coherence

Adam Eaton,[1] Dibya Mukherjee,[1] and H. A. Fertig[1,2]
[1]*Department of Physics, Indiana University, Bloomington, Indiana 47405, USA*
[2]*Quantum Science and Engineering Center, Indiana University, Bloomington, Indiana 47405, USA*

(Received 12 January 2024; revised 24 June 2024; accepted 26 June 2024; published 11 July 2024)

Lifshitz transitions are topological transitions of a Fermi surface, whose signatures typically appear in the conduction properties of a host metal. Here, we demonstrate, using an extended Falicov-Kimball model of a two-flavor fermion system, that a Lifshitz transition which occurs in the noninteracting limit impacts interaction-induced insulating phases, even though they do not host Fermi surfaces. For strong interactions we find a first-order transition between states of different polarization. This transition line ends in a very unusual quantum critical endpoint, whose presence is stabilized by the onset of interflavor coherence. We demonstrate that the surfaces of maximum coherence in these states reflect the distinct Fermi-surface topologies of the states separated by the noninteracting Lifshitz transition. Experimental realizations of our results are discussed for both electronic and optical lattice systems.

DOI: 10.1103/PhysRevB.110.035132

I. INTRODUCTION

In recent years, topology has become increasingly appreciated in condensed matter physics as a framework for understanding diverse physical phenomena. These include the Thouless pump [1,2], topological defects [3–9], quantized Hall effects [10–18], magnetic breakdown [19–22], and topological insulators [23–33]. In addition to its utility for theoretical understanding, topology is physically significant because it leads to phenomena that are robust with respect to various perturbations [34–38].

Lifshitz transitions [39–44] are an example of this. They occur when the topology of a Fermi surface changes with system parameters such as pressure, doping, or external magnetic field [40–42,44], and typically are observable as anomalies in magneto-oscillation periods as the system passes through such transitions. Because a Lifshitz transition is a Fermi-surface phenomenon, its impact is normally only expected in metallic systems. In this paper, we demonstrate that such transitions can also impact systems when spontaneous symmetry breaking takes them outside their metallic regime, leaving a clear and unique signature in the phase diagram.

To show this, we examine a two-flavor system with interactions such that interflavor coherent phases can be supported. This system supports different phases where the loops of maximum coherence in the Brillouin zone are topologically distinct. An example of this is presented in Fig. 1. The topologies of the Fermi surfaces on either side of the Lifshitz transition mirror the topologies of these maximum coherence loops, demonstrating that the Lifshitz transition "seeds" the quantum phase transition of the interacting system. Importantly, the two different coherent states are separated by a first-order transition for relatively strong interactions. Most surprisingly, within the models we examine, the transition line ends at a *quantum critical endpoint* (QCEP) [45], reminiscent of a thermodynamic $\mathcal{Z}_2$ critical point [9,46]. Beyond the endpoint the evolution between coherent phases becomes continuous, with no sharp distinction between the states. An example of a phase diagram with such a QCEP is illustrated in Fig. 1(c). As we explain below, the presence of the QCEP results directly from the interplay of the changing Fermi-surface topology associated with a noninteracting Lifshitz transition, and the tendency towards spontaneous symmetry breaking in interacting multicomponent systems at zero temperature.

The QCEP structure we find is relatively robust: For example, it is present both in systems where the first-order line separates states which are both trivial, and ones in which one of the two states is topological [47,48]. We find that the first-order line for strong interactions can separate states of different topologies, but near the QCEP, states on either side of the transition are always topologically equivalent. As we discuss below, this phenomenology is in principle relevant to multicomponent electron systems, including ones in which populations of spin, valley, or layer index can vary, as well as in optical lattice systems hosting more than one species of fermionic atoms.

II. MODEL HAMILTONIAN

Our study focuses on a minimal model which captures the physics of interest, while allowing some flexibility to demonstrate its generality across different types of bands. The noninteracting part of our Hamiltonian is a Bernevig-Hughs-Zhang (BHZ) model [17], which supports nontrivial band topology [29–33]. The electrons have a flavor index ℓ for which we allow two values, and at momentum $\mathbf{k}$ this Hamiltonian is

$$h_{\ell,\boldsymbol{k}} = s_\ell(\hbar v \sin k_x \sigma_x + \hbar v \sin k_y \sigma_y + M_{\ell,\boldsymbol{k}}\sigma_z) + \Delta_\ell \mathbb{1}, \quad (1)$$

where $s_\ell = \pm 1$ is an index used to fix the Chern numbers of the lowest-energy bands, the lattice constant $a = 1$, Δ_ℓ is a flavor-dependent potential which we set to Δ for one flavor and $-\Delta$ for the other, σ_i ($i \in \{x, y, z\}$) are Pauli matrices acting on two internal orbitals associated with each tight-binding

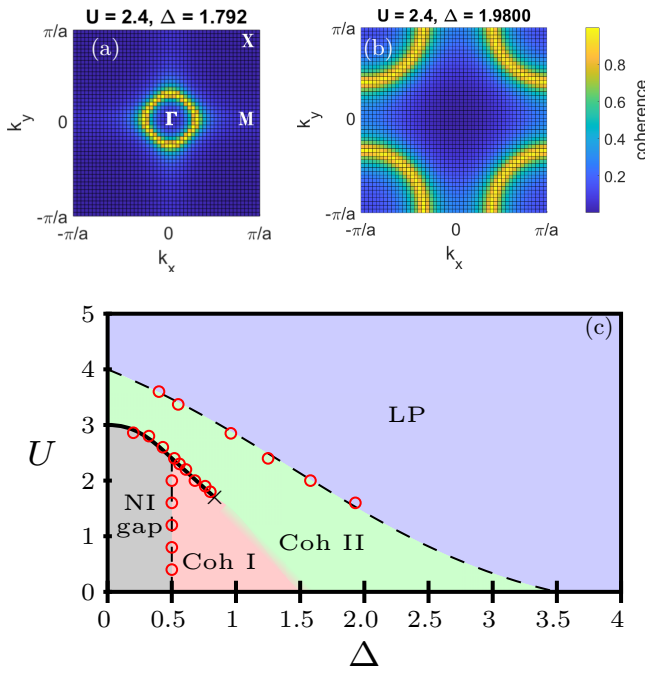

FIG. 1. (a), (c) Interflavor coherence as a function of crystal momentum, for interaction strengths U and biases Δ on either side of the first-order transition line. Regions of largest coherence form closed loops which surround either the center or corner of the Brillouin zone, with a sharp change in this topology. The BZ high-symmetry points Γ, M, and X are labeled. (b) Phase diagram for the model defined by Eq. (2). Open circles represent numerical results; lines are guides to the eye. The solid line indicates first-order transition; dashed lines are continuous transitions. $\times$ indicates the position of QCEP. Phases include one continuously connected to a noninteracting gap phase (NIG); two distinct coherent phases Coh I and Coh II, distinguished by the topologies of their maximum coherence loops, and a polarized phase (LP) in which all the fermions are in the same discrete state.

site, and v is the Fermi velocity. In units where $\hbar v = 1$, $M_{\ell,\boldsymbol{k}} = m_\ell + 2 - \cos k_x - \cos k_y$. For $-4 < m_\ell < 0$, the two bands of each flavor have a Chern number $\mathcal{C} = \pm 1$; outside this interval their Chern numbers are zero. For simplicity we take $m_\ell = -0.5$, and we focus on total fermion densities such that the system is at half filling. Occupation of the two flavors of electrons is controlled by varying the bias parameter Δ, and we focus on ranges of this parameter such that (in the absence of interactions) the lower-energy band of one flavor crosses the upper energy band of the other.

For $\Delta_\ell = 0$ this Hamiltonian has eigenvalues $E_{\boldsymbol{k}} = \sqrt{\sin^2 k_x + \sin^2 k_y + M_{\boldsymbol{k}}^2}$ and corresponding eigenstates $\chi_{\mathbf{k},\pm 1}$ [see Supplemental Material (SM) [49] for concrete forms]. It terms of these, the interacting model we study is

$$\hat{H} = \sum_{\mathbf{k}} \sum_{\ell} \sum_{p=\pm 1} [pE_{\boldsymbol{k}} + \Delta_\ell] \hat{c}^\dagger_{\mathbf{k},\ell,p} \hat{c}_{\mathbf{k},\ell,p} + U \sum_{\mathbf{k}} \hat{\rho}_{-\boldsymbol{k},t} \hat{\rho}_{\boldsymbol{k},b}, \tag{2}$$

where $\hat{c}^\dagger_{\mathbf{k},\ell,p=\pm 1}$ creates a particle in an eigenstate of $h_{\ell,\mathbf{k}}$ with energy $pE_{\mathbf{k}} + \Delta_\ell$. The second term is an interlayer contact interaction [16,30] that involves density operators $\hat{\rho}_{\boldsymbol{k},\ell} = \sum_{\mathbf{q},p=\pm 1} \chi^\dagger_{\mathbf{k}+\mathbf{q},p} \cdot \chi_{\mathbf{q},p} \hat{c}^\dagger_{\mathbf{q}+\mathbf{k},\ell,p} \hat{c}_{\mathbf{q},\ell,p}$. Equation (2) preserves the total number of fermions of each flavor separately, thus supporting a $U(1)$ flavor symmetry. Such models belong to the general class of extended Falicov-Kimball models (EFKM), which have been studied as candidates for describing electronic bilayers, excitonic physics, and ferroelectricity [50–59].

The model can be interpreted as a bilayer system without tunneling between layers [60–63]), in which intralayer interactions have been neglected. In what follows we adopt this realization as a paradigm for such systems, and refer to the flavors as layers, with t and b in Eq. (2) denoting the top and bottom layers. We expect the behavior of this model at half filling to apply when bands of each flavor are relatively far apart energetically, while there is a crossing of bands of two different flavors: With short-range interactions, Fermi statistics suppresses short-range intraflavor interactions, allowing interflavor interactions to dominate. Beyond this, the model can also be mapped onto a two-species fermionic atomic gas system in an optical lattice, as we discuss below.

III. HARTREE-FOCK ANALYSIS

We consider ground states of $\hat{H}$ within the Hartree-Fock (HF) approximation, in situations where the system is half filled. Details of the analysis may be found in the SM [49]. For $\Delta = 0$ (implying flavor-degenerate bands), the spectrum consists of one filled and one empty band for each layer, with an intervening gap that is present even in the absence of interactions. With increasing $|\Delta|$, bands from different layers approach one another, eventually crossing when spontaneous symmetry breaking is not considered [49]. The Fermi surfaces consist of matching loops in each layer, surrounding the Γ point of the square Brillouin zone (BZ). With growing $|\Delta|$ these loops eventually touch the M points at the BZ edge, signaling a Lifshitz transition. For still larger $|\Delta|$ the loop topology changes, now surrounding the X points (corners) of the BZ [49].

Multiflavor systems with matching Fermi surfaces are known to be unstable to spontaneous interflavor coherence in the presence of interactions [64,65]. Figure 1(b) illustrates the phase diagram, within our HF analysis, when two bands pass fully through one another as a function of Δ for the situation $s_{\ell=t} = -s_{\ell=b}$ in Eq. (1), for which the crossing bands have the same Chern number. Results for $s_t = s_b$ are qualitatively similar, as discussed in the SM [49]. The resulting phases include a noninteracting gap (NIG) phase, which is continuously connected to the $\Delta = 0$ noninteracting state; interlayer coherent phases (Coh I and II); and a layer-polarized (LP) phase. Continuous transitions are indicated as dashed lines while solid lines indicate first-order transitions.

Two types of order are important in characterizing the phases. The first is a layer polarization, which we quantify with a polarization function $P(\boldsymbol{k}) \equiv \sum_{i=1}^4 \langle \psi_i(\boldsymbol{k}) | \tau_z \otimes \mathbb{1} | \psi_i(\boldsymbol{k}) \rangle f(E_i^{\mathrm{HF}}(\boldsymbol{k})) \equiv \sum_{i=1}^4 P_i(\boldsymbol{k}) f(E_i^{\mathrm{HF}}(\boldsymbol{k}))$, where $|\psi_i(\mathbf{k})\rangle$ are the four HF wave functions at wave vector $\mathbf{k}$ with energy $E_i^{\mathrm{HF}}(\mathbf{k})$, f is the Fermi function, and τ_z is a Pauli matrix acting in layer space. Spontaneous coherence in the system arises

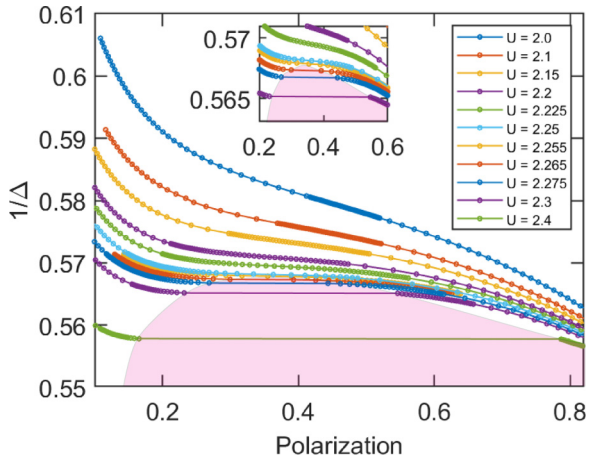

FIG. 2. Plot of P vs $1/\Delta$ for different values of U, illustrating a discontinuous polarization jump which gets smaller as the QCEP is approached. Inset: Detail of the polarization jump near QCEP.

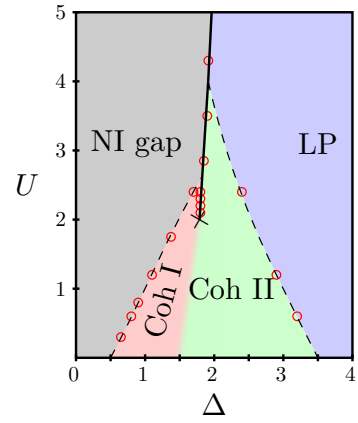

FIG. 3. Phase diagram for the two-band model. Open circles represent numerical results; lines are guides to the eye. Dashed lines are represent continuous transitions, and the solid line is a first-order transition, ending at a QCEP, indicated by the × symbol.

when order parameters of the form $\langle c^\dagger_{\mathbf{k},\ell,p} c_{\mathbf{k},\ell',p'}\rangle \neq 0$ for $\ell \neq \ell'$. This always entails values of $P_i(\mathbf{k})$ which are not equal to either -1 or 1, so that nonvanishing values of a coherence function, $C(\boldsymbol{k}) \equiv \sum_k \sum_{i=1}^4 (1 - |P_i(\boldsymbol{k})|) f(E_i^{\rm HF}(\boldsymbol{k}))$, signal the presence of interlayer coherence.

Figures 1(a) and 1(b) illustrate the behavior of $C(\mathbf{k})$ as a function of $\mathbf{k}$ for two coherent states on opposite sides of a first-order transition. The loci of maximum $C(\mathbf{k})$ have two different topologies, reflecting the behavior of the Fermi surfaces on either side of the noninteracting Lifshitz transition. For small U the evolution from one behavior to the other as a function of Δ is continuous, while for larger values there is a first-order transition between them. The transition line is quite interesting, and its behavior represents a main point of our study. It hosts a very unusual QCEP, which at the mean-field level is highly analogous to the critical point of a thermal $\mathcal{Z}_2$ transition. Indeed, the behavior of the full polarization, $P = \sum_{\mathbf{k}} P(\mathbf{k})$, when the bias Δ is varied, displays a jump that continuously vanishes at the QCEP, as illustrated in Fig. 2. This behavior is highly analogous to that of, for example, the density jump in a thermal liquid-gas transition [66].

IV. TWO-BAND MODEL

To understand the origin of the QCEP and its connection to the noninteracting Lifshitz transition, it is convenient to simplify this system to a two-band model, in which only the bands that cross one another as a function of Δ are retained. These can have the same or opposite topologies; for simplicity we discuss the former case, although results in the latter case are quite similar. Figure 3 illustrates the resulting phase diagram. Although there is a change in the locations of the phase boundaries, particularly at large U, the system retains the same basic phases and features of the four-band model. Most prominent is the first-order transition line dropping from large U, ending at a QCEP.

The phases of this model are characterized by two order parameters: (i) $B_p \equiv \frac{U}{2V}\sum_{\mathbf{k}} \langle \hat{c}^\dagger_{\mathbf{k},t} \hat{c}_{\mathbf{k},t} - \hat{c}^\dagger_{\mathbf{k},b} \hat{c}_{\mathbf{k},b}\rangle$, where $\hat{c}_{\mathbf{k},\ell}$ annihilates a particle in the retained band of layer ℓ, which is a measure of the polarization of the system; and (ii) an interlayer coherence $B^{tb}(\mathbf{k}) \equiv \frac{U}{V}\sum_{\mathbf{k}_1} |\chi^\dagger_{\mathbf{k},t} \cdot \chi_{\mathbf{k}_1,b}|^2 \langle c^\dagger_{\mathbf{k}_1,t} c_{\mathbf{k}_1,b}\rangle$. ($V$ is the system area.) Defining $\tilde{\xi}(\mathbf{k}) = E_{\mathbf{k}} + \Delta + B_p$, the mean-field self-consistent equations for these have the form [49]

$$\frac{B_p}{U} = \frac{1}{2V}\sum_{\mathbf{k}_2} \frac{\tilde{\xi}(\mathbf{k}_2)}{\sqrt{|\tilde{\xi}(\mathbf{k}_2)|^2 + |B^{tb}(\mathbf{k}_2)|^2}} \equiv F(B_p + \Delta), \quad (3)$$

$$B^{tb}(\mathbf{k}_1) = \frac{U}{2V}\sum_{\mathbf{k}_2} \frac{(\cos^2\theta_{\mathbf{k}_1}/2)(\cos^2\theta_{\mathbf{k}_2}/2) B^{tb}(\mathbf{k}_2)}{\sqrt{|\tilde{\xi}(\mathbf{k}_2)|^2 + |B^{tb}(\mathbf{k}_2)|^2}}, \quad (4)$$

where $\tilde{\xi}(\mathbf{k}_2) = E_{\mathbf{k}_2} + \Delta + B_p$, and, setting m_ℓ to the same value for both layers, so that $M_{\ell,\mathbf{k}} \equiv M_{\mathbf{k}}$ is independent of the layer index, $\cos\theta_{\mathbf{k}}/2 = (E_{\mathbf{k}} + M_{\mathbf{k}})/\sqrt{2E_{\mathbf{k}}(E_{\mathbf{k}} + M_{\mathbf{k}})}$ [49]. In Eq. (4) we have assumed that $\langle c^\dagger_{\mathbf{k}_1,t} c_{\mathbf{k}_1,b}\rangle$ is real and has C_4 rotational symmetry in the HF ground state, as we indeed find in our more general numerical analysis.

Equation (3) provides particular insight into the connection between the first-order transition line in Fig. 3 and a thermal $\mathcal{Z}_2$ transition. Figure 4 illustrates the left-hand side (B_p/U) and right-hand side $[F(B_p + \Delta)]$ of the equation, with solutions occurring where they cross. At large positive (negative) values of the bias parameter Δ, one finds a single solution with maximal negative (positive) values of B_p, while in a transition region there are three solutions. The physical state of the system jumps between two of the three solutions with changing Δ, when their energies cross. This behavior is highly reminiscent of what one finds in a mean-field treatment of, for example, the liquid-gas transition [66]. The jump is always present at some Δ provided $\max_x \frac{dF(x)}{dx} > \frac{1}{U}$.

There is a remarkable relationship between the Lifshitz transition and behavior of the first-order transition. Consider the situation for states with $B^{tb} = 0$. It is not difficult to show in this case that the slope of $F(B_p + \Delta)$ in Eq. (3) *diverges* at $B_p + \Delta = 0$. The origin of this divergence is precisely the Lifshitz transition itself: The change in Fermi-surface topology leads directly to this singularity. In this situation, $\max_x \frac{dF(x)}{dx} = \infty$, and, for $U = 0$, the first-order transition line

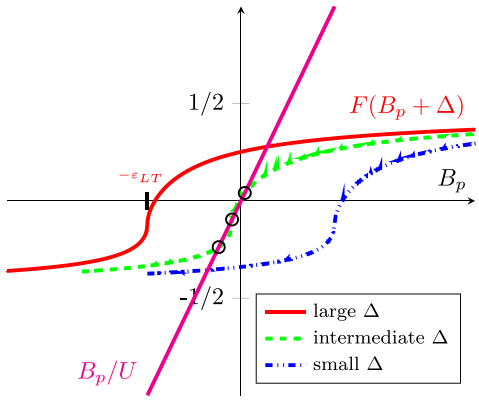

FIG. 4. Left- and right-hand (RH) sides of Eq. (3) for different values of Δ, for $B^{tb}=0$. For small and large Δ the curves cross once, while for intermediate Δ they cross three times. Circles indicate solutions to the self-consistent equation at intermediate Δ. The existence of three solutions indicates a first-order transition. Because of the Lifshitz transition (energy indicated by $-\varepsilon_{\rm LT}$ for the lowest Δ), a divergence occurs in the slope of the RH side curve, yielding a first-order transition for arbitrarily small U. Coherence ($B^{tb}\neq 0$) lowers this maximum slope to a finite value, eliminating the first-order transition at small U and stabilizing the QCEP.

will end precisely at the Lifshitz transition point. In this situation there is no QCEP. This is what one commonly finds in zero-temperature phase diagrams of multicomponent fermion systems [67–70]. Figure 4 illustrates how Eq. (3) generates a first-order jump for any positive value of U.

Interlayer coherence (i.e., $|B^{tb}|>0$) changes this phenomenology. A nonvanishing B^{tb} smooths the integrand in Eq. (3) and lifts the divergence in $F(x)$. Because $\max_x \frac{dF(x)}{dx} < \infty$ in this situation, for sufficiently small (but nonvanishing) U there will be only *one* solution to Eq. (3). Thus for small U, the first-order jump gives way to a continuous crossover, whereas it is still present for larger values of U. In this way, a QCEP is stabilized.

The phenomenology of Eq. (3) bears a strong similarity to what one finds in classical mean-field theories, for example, in the finite-temperature theory of the liquid-gas transition [66]. In such settings, a critical point at the end of a first-order transition line is a well-known and important physical phenomenon. Remarkably, in order to be realized in this zero-temperature setting, spontaneous coherence, a purely quantum phenomenon, must be manifested between layers.

V. DISCUSSION

The impact of the Lifshitz transition on the phase diagram of an interacting system applies beyond the specific model we have discussed. For example, one may consider different topologies of crossing bands which host Lifshitz transitions. We find that the appearance of a QCEP is again manifested, although details of the coherence onset, as well as the evolution of the band topology, differ in interesting ways. This is discussed more fully in the SM [49].

The phases of multiflavor fermion systems and the transitions among them are relevant to a broad range of fermion systems, including magnets [45,68,71,72], exciton condensates [73–76], bilayer electron systems [67,77–80], and multicomponent quantum Hall systems [81–85]. In the vast majority of cases, nothing analogous to the QCEP we find arises. Two exceptions are metallic ferromagnets [45], where gapless fermion excitations help stabilize a QCEP, and interacting topological systems [47,75,86], in which a first-order topological transition line evolves into a second-order one. In both cases, fluctuations are key to stabilizing a critical point. By contrast, our study uncovers a very different path to a QCEP, seeded by the proximity of a Lifshitz transition, and stabilized by the onset of interflavor coherence. It arises already at the mean-field level.

These results suggest a number of interesting questions. For example, the presence of a broken $U(1)$ symmetry and its accompanying Goldstone mode in the vicinity of the QCEP suggests that its critical behavior will be different than that of a classical thermal $\mathcal{Z}_2$ transition. Effects of real thermal fluctuations on the system, and the form a quantum critical region [87,88] takes, are important to understand in settings where temperature effects cannot be ignored. Another set of questions involve how the specific system we have studied might be physically manifested. One interesting possibility involves an optical lattice [89] hosting two species of atoms with an interspecies Feshbach resonance [90,91]. A particle-hole transformation maps this onto an EFKM; under such a transformation, superconductivity manifested by the system is equivalent to interflavor coherence of the states discussed above. Indeed, the parameter B^{tb} essentially becomes the superconducting gap function under the particle-hole transformation. For appropriate parameters, we expect *two* states, with different solutions for the superconducting gap, separated by a first-order transition. Beyond this, van der Waals materials [92] offer platforms for electron bilayer realizations of this system, which support layer polarized states [93,94] and/or interlayer coherence [85,95–98], whose interaction and competition could lead to novel quantum phase boundaries and transitions such as those we have described in this paper.

ACKNOWLEDGMENTS

The authors acknowledge useful discussions with Chunli Huang, Ganpathy Murthy, and Phil Richerme. This research was supported in part by Lilly Endowment, Inc., through its support for the Indiana University Pervasive Technology Institute. This work is supported in part by NSF Grants No. DMR-1914451 and No. ECCS-1936406. The authors thank the Aspen Center for Physics (NSF Grant No. PHY-1607611) where part of this work was done.

[1] Y. E. Kraus, Y. Lahini, Z. Ringel, M. Verbin, and O. Zilberberg, Topological states and adiabatic pumping in quasicrystals, Phys. Rev. Lett. **109**, 106402 (2012).

[2] K. A. Madsen, E. J. Bergholtz, and P. W. Brouwer, Topological equivalence of crystal and quasicrystal band structures, Phys. Rev. B **88**, 125118 (2013).

[3] Z. Ringel, Y. E. Kraus, and A. Stern, Strong side of weak topological insulators, Phys. Rev. B **86**, 045102 (2012).

[4] J. C. Y. Teo and T. L. Hughes, Existence of Majorana-fermion bound states on disclinations and the classification of topological crystalline superconductors in two dimensions, Phys. Rev. Lett. **111**, 047006 (2013).

[5] M. Veldhorst, M. Snelder, M. Hoek, T. Gang, V. K. Guduru, X. L. Wang, U. Zeitler, W. G. van der Wiel, A. A. Golubov, H. Hilgenkamp, and A. Brinkman, Josephson supercurrent through a topological insulator surface state, Nat. Mater. **11**, 417 (2012).

[6] L. Fu and C. L. Kane, Superconducting proximity effect and Majorana fermions at the surface of a topological insulator, Phys. Rev. Lett. **100**, 096407 (2008).

[7] L. Fu and C. L. Kane, Josephson current and noise at a superconductor/quantum-spin-Hall-insulator/superconductor junction, Phys. Rev. B **79**, 161408(R) (2009).

[8] D. R. Nelson, *Defects and Geometry in Condensed Matter Physics* (Cambridge University Press, Cambridge, UK, 2002).

[9] P. M. Chaikin, T. C. Lubensky, and T. A. Witten, *Principles of Condensed Matter Physics* (Cambridge University Press, Cambridge, UK, 1995), Vol. 10.

[10] D. J. Thouless, M. Kohmoto, M. P. Nightingale, and M. den Nijs, Quantized Hall conductance in a two-dimensional periodic potential, Phys. Rev. Lett. **49**, 405 (1982).

[11] J. I. Väyrynen, M. Goldstein, and L. I. Glazman, Helical edge resistance introduced by charge puddles, Phys. Rev. Lett. **110**, 216402 (2013).

[12] S. Hart, H. Ren, T. Wagner, P. Leubner, M. Mühlbauer, C. Brüne, H. Buhmann, L. W. Molenkamp, and A. Yacoby, Induced superconductivity in the quantum spin Hall edge, Nat. Phys. **10**, 638 (2014).

[13] C. Weeks, J. Hu, J. Alicea, M. Franz, and R. Wu, Engineering a robust quantum spin Hall state in graphene via adatom deposition, Phys. Rev. X **1**, 021001 (2011).

[14] C.-Y. Hou, E.-A. Kim, and C. Chamon, Corner junction as a probe of helical edge states, Phys. Rev. Lett. **102**, 076602 (2009).

[15] L. Du, I. Knez, G. Sullivan, and R.-R. Du, Robust helical edge transport in gated InAs/GaSb bilayers, Phys. Rev. Lett. **114**, 096802 (2015).

[16] A. M. Bozkurt, B. Pekerten, and İ. Adagideli, Work extraction and Landauer's principle in a quantum spin Hall device, Phys. Rev. B **97**, 245414 (2018).

[17] B. A. Bernevig, T. L. Hughes, and S.-C. Zhang, Quantum spin Hall effect and topological phase transition in HgTe quantum wells, Science **314**, 1757 (2006).

[18] S. Girvin and K. Yang, *Modern Condensed Matter Physics* (Cambridge University Press, Cambridge, UK, 2019).

[19] C.-K. Lu and H. A. Fertig, Magnetic breakdown in twisted bilayer graphene, Phys. Rev. B **89**, 085408 (2014).

[20] R. Chapai, M. Leroux, V. Oliviero, D. Vignolles, N. Bruyant, M. P. Smylie, D. Y. Chung, M. G. Kanatzidis, W.-K. Kwok, J. F. Mitchell, and U. Welp, Magnetic breakdown and topology in the kagome superconductor CsV_3Sb_5 under high magnetic field, Phys. Rev. Lett. **130**, 126401 (2023).

[21] A. Alexandradinata and L. Glazman, Geometric phase and orbital moment in quantization rules for magnetic breakdown, Phys. Rev. Lett. **119**, 256601 (2017).

[22] G. Lemut, A. D. Vela, M. J. Pacholski, J. Tworzydło, and C. W. J. Beenakker, Magnetic breakdown spectrum of a Kramers-Weyl semimetal, New J. Phys. **22**, 093022 (2020).

[23] M. Z. Hasan and C. L. Kane, *Colloquium:* Topological insulators, Rev. Mod. Phys. **82**, 3045 (2010).

[24] X.-L. Qi and S.-C. Zhang, Topological insulators and superconductors, Rev. Mod. Phys. **83**, 1057 (2011).

[25] N. R. Cooper and R. Moessner, Designing topological bands in reciprocal space, Phys. Rev. Lett. **109**, 215302 (2012).

[26] J. Wang, B. Lian, and S.-C. Zhang, Quantum anomalous Hall effect in magnetic topological insulators, Phys. Scr. **T164**, 014003 (2015).

[27] T. Neupert, L. Santos, C. Chamon, and C. Mudry, Fractional quantum Hall states at zero magnetic field, Phys. Rev. Lett. **106**, 236804 (2011).

[28] S. Rachel, Quantum phase transitions of topological insulators without gap closing, J. Phys.: Condens. Matter **28**, 405502 (2016).

[29] Y. Ren, Z. Qiao, and Q. Niu, Engineering corner states from two-dimensional topological insulators, Phys. Rev. Lett. **124**, 166804 (2020).

[30] A. M. Lunde and G. Platero, Hyperfine interactions in two-dimensional HgTe topological insulators, Phys. Rev. B **88**, 115411 (2013).

[31] R. Seshadri, A. Dutta, and D. Sen, Generating a second-order topological insulator with multiple corner states by periodic driving, Phys. Rev. B **100**, 115403 (2019).

[32] C.-X. Liu, X.-L. Qi, H. J. Zhang, X. Dai, Z. Fang, and S.-C. Zhang, Model Hamiltonian for topological insulators, Phys. Rev. B **82**, 045122 (2010).

[33] J. K. Asbóth, L. Oroszlány, and A. Pályi, Time-reversal symmetric two-dimensional topological insulators: The Bernevig–Hughes–Zhang model, in *A Short Course on Topological Insulators: Band Structure and Edge States in One and Two Dimensions* (Springer International Publishing, Cham, 2016), pp. 119–138.

[34] C. Nayak, S. H. Simon, A. Stern, M. Freedman, and S. Das Sarma, Non-Abelian anyons and topological quantum computation, Rev. Mod. Phys. **80**, 1083 (2008).

[35] M. Lohse, C. Schweizer, H. M. Price, O. Zilberberg, and I. Bloch, Exploring 4D quantum Hall physics with a 2D topological charge pump, Nature (London) **553**, 55 (2018).

[36] B. Hu, Z. Zhang, H. Zhang, L. Zheng, W. Xiong, Z. Yue, X. Wang, J. Xu, Y. Cheng, X. Liu, and J. Christensen, Non-Hermitian topological whispering gallery, Nature (London) **597**, 655 (2021).

[37] A. Abanov, Topology, geometry and quantum interference in condensed matter physics, in *Topology and Condensed Matter Physics*, edited by S. M. Bhattacharjee, M. Mj, and A. Bandyopadhyay (Springer, Singapore, 2017), pp. 281–331.

[38] A. Hamma, L. Cincio, S. Santra, P. Zanardi, and L. Amico, Local response of topological order to an external perturbation, Phys. Rev. Lett. **110**, 210602 (2013).

[39] G. E. Volovik, Exotic Lifshitz transitions in topological materials, Phys. Usp. **61**, 89 (2018).

[40] Y. Li, A. Eaton, H. A. Fertig, and B. Seradjeh, Dirac magic and Lifshitz transitions in AA-stacked twisted multilayer graphene, Phys. Rev. Lett. **128**, 026404 (2022).

[41] K.-S. Chen, Z. Y. Meng, T. Pruschke, J. Moreno, and M. Jarrell, Lifshitz transition in the two-dimensional Hubbard model, Phys. Rev. B **86**, 165136 (2012).

[42] Y. Lemonik, I. L. Aleiner, C. Toke, and V. I. Fal'ko, Spontaneous symmetry breaking and Lifshitz transition in bilayer graphene, Phys. Rev. B **82**, 201408(R) (2010).
[43] R. S. Akzyanov, Lifshitz transition in dirty doped topological insulator with nematic superconductivity, Phys. Rev. B **104**, 224502 (2021).
[44] L. Balents and O. A. Starykh, Quantum Lifshitz field theory of a frustrated ferromagnet, Phys. Rev. Lett. **116**, 177201 (2016).
[45] M. Brando, D. Belitz, F. M. Grosche, and T. R. Kirkpatrick, Metallic quantum ferromagnets, Rev. Mod. Phys. **88**, 025006 (2016).
[46] A. Pelissetto and E. Vicari, Critical phenomena and renormalization-group theory, Phys. Rep. **368**, 549 (2002).
[47] A. Amaricci, J. C. Budich, M. Capone, B. Trauzettel, and G. Sangiovanni, First-order character and observable signatures of topological quantum phase transitions, Phys. Rev. Lett. **114**, 185701 (2015).
[48] V. Juričić, D. S. L. Abergel, and A. V. Balatsky, First-order quantum phase transition in three-dimensional topological band insulators, Phys. Rev. B **95**, 161403(R) (2017).
[49] See Supplemental Material at http://link.aps.org/supplemental/10.1103/PhysRevB.110.035132 for here we provide details of our self-consistent equations and further details about the topological transition. For the self-consistent equations, we show the calculations of B^{tb} (i.e., the coherence) and demonstrate how the results depend on the topology of the bands. We also provide further numerical and analytic analysis on the system's behavior near topological transitions.
[50] C. D. Batista, Electronic ferroelectricity in the Falicov-Kimball model, Phys. Rev. Lett. **89**, 166403 (2002).
[51] J. K. Freericks and V. Zlatić, Exact dynamical mean-field theory of the Falicov-Kimball model, Rev. Mod. Phys. **75**, 1333 (2003).
[52] C. D. Batista, J. E. Gubernatis, J. Bonča, and H. Q. Lin, Intermediate coupling theory of electronic ferroelectricity, Phys. Rev. Lett. **92**, 187601 (2004).
[53] D. Ihle, M. Pfafferott, E. Burovski, F. X. Bronold, and H. Fehske, Bound state formation and the nature of the excitonic insulator phase in the extended Falicov-Kimball model, Phys. Rev. B **78**, 193103 (2008).
[54] V.-N. Phan, H. Fehske, and K. W. Becker, Excitonic resonances in the 2D extended Falicov-Kimball model, Europhys. Lett. **95**, 17006 (2011).
[55] D. I. Golosov, Collective excitations and stability of the exciton phase in the extended Falicov-Kimball model, Phys. Rev. B **86**, 155134 (2012).
[56] B. Zenker, D. Ihle, F. X. Bronold, and H. Fehske, Electron-hole pair condensation at the semimetal-semiconductor transition: A BCS-BEC crossover scenario, Phys. Rev. B **85**, 121102(R) (2012).
[57] T. Kaneko, S. Ejima, H. Fehske, and Y. Ohta, Exact-diagonalization study of exciton condensation in electron bilayers, Phys. Rev. B **88**, 035312 (2013).
[58] S. Ejima, T. Kaneko, Y. Ohta, and H. Fehske, Order, criticality, and excitations in the extended Falicov-Kimball model, Phys. Rev. Lett. **112**, 026401 (2014).
[59] P. Farkašovský, Hartree-Fock exploration of electronic ferroelectricity, valence transitions, and metal-insulator transitions in the extended Falicov-Kimball model, Phys. Rev. B **108**, 075161 (2023).
[60] L. Zheng, M. W. Ortalano, and S. Das Sarma, Exchange instabilities in semiconductor double-quantum-well systems, Phys. Rev. B **55**, 4506 (1997).
[61] C. B. Hanna, D. Haas, and J. C. Díaz-Vélez, Double-layer systems at zero magnetic field, Phys. Rev. B **61**, 13882 (2000).
[62] T. Cookmeyer and S. Das Sarma, Symmetry breaking in zero-field two-dimensional electron bilayers, Phys. Rev. B **109**, 115307 (2024).
[63] J. Zhu and S. Das Sarma, Interaction and coherence in two-dimensional bilayers, Phys. Rev. B **109**, 085129 (2024).
[64] H. Min, R. Bistritzer, J.-J. Su, and A. H. MacDonald, Room-temperature superfluidity in graphene bilayers, Phys. Rev. B **78**, 121401(R) (2008).
[65] B. Seradjeh, J. E. Moore, and M. Franz, Exciton condensation and charge fractionalization in a topological insulator film, Phys. Rev. Lett. **103**, 066402 (2009).
[66] R. Pathria and P. D. Beale, *Statistical Mechanics*, 4th ed. (Academic Press, San Diego, 2022).
[67] M. M. Fogler, L. V. Butov, and K. S. Novoselov, High-temperature superfluidity with indirect excitons in van der Waals heterostructures, Nat. Commun. **5**, 4555 (2014).
[68] S. Miyakoshi and Y. Ohta, Coexistence of magnetic and topological phases in the asymmetric Kane-Mele-Hubbard model, J. Phys.: Conf. Ser. **592**, 012129 (2015).
[69] J.-J. Su and A. H. MacDonald, Spatially indirect exciton condensate phases in double bilayer graphene, Phys. Rev. B **95**, 045416 (2017).
[70] M. Xie, H. Pan, F. Wu, and S. Das Sarma, Nematic excitonic insulator in transition metal dichalcogenide moiré heterobilayers, Phys. Rev. Lett. **131**, 046402 (2023).
[71] N. Bultinck, S. Chatterjee, and M. P. Zaletel, Mechanism for anomalous Hall ferromagnetism in twisted bilayer graphene, Phys. Rev. Lett. **124**, 166601 (2020).
[72] Q. H. Wang, A. Bedoya-Pinto, M. Blei, A. H. Dismukes, A. Hamo, S. Jenkins, M. Koperski, Y. Liu, Q.-C. Sun, E. J. Telford, H. H. Kim, M. Augustin, U. Vool, J.-X. Yin, L. H. Li, A. Falin, C. R. Dean, F. Casanova, R. F. L. Evans, M. Chshiev *et al.*, The magnetic genome of two-dimensional van der Waals materials, ACS Nano **16**, 6960 (2022).
[73] J. F. Jan and Y. C. Lee, Bose-Einstein condensation of excitons in two dimensions, Phys. Rev. B **58**, R1714 (1998).
[74] D. Wang, N. Luo, W. Duan, and X. Zou, High-temperature excitonic Bose–Einstein condensate in centrosymmetric two-dimensional semiconductors, J. Phys. Chem. Lett. **12**, 5479 (2021).
[75] A. Amaricci, G. Mazza, M. Capone, and M. Fabrizio, Exciton condensation in strongly correlated quantum spin Hall insulators, Phys. Rev. B **107**, 115117 (2023).
[76] Q. Gao, Y.-h. Chan, Y. Wang, H. Zhang, P. Jinxu, S. Cui, Y. Yang, Z. Liu, D. Shen, Z. Sun, J. Jiang, T. C. Chiang, and P. Chen, Evidence of high-temperature exciton condensation in a two-dimensional semimetal, Nat. Commun. **14**, 994 (2023).
[77] M. Kharitonov, Antiferromagnetic state in bilayer graphene, Phys. Rev. B **86**, 195435 (2012).
[78] Y. Zhang, K. Jiang, Z. Wang, and F. Zhang, Correlated insulating phases of twisted bilayer graphene at commensurate filling fractions: A Hartree-Fock study, Phys. Rev. B **102**, 035136 (2020).
[79] X. Li, X. Xu, H. Zhou, H. Jia, E. Wang, H. Fu, J.-T. Sun, and S. Meng, Tunable topological states in

stacked Chern insulator bilayers, Nano Lett. **23**, 2839 (2023).

[80] G. Shavit, K. c. v. Kolář, C. Mora, F. von Oppen, and Y. Oreg, Strain disorder and gapless intervalley coherent phase in twisted bilayer graphene, Phys. Rev. B **107**, L081403 (2023).

[81] H. A. Fertig, Energy spectrum of a layered system in a strong magnetic field, Phys. Rev. B **40**, 1087 (1989).

[82] S. Das Sarma, S. Sachdev, and L. Zheng, Double-layer quantum Hall antiferromagnetism at filling fraction $\nu 2/m$ where m is an odd integer, Phys. Rev. Lett. **79**, 917 (1997).

[83] *Perspectives in Quantum Hall Effects*, edited by S. Das Sarma and A. Pinczuk (Wiley-VCH, Weinheim, Germany, 2008).

[84] A. Kumar, R. Roy, and S. L. Sondhi, Generalizing quantum Hall ferromagnetism to fractional Chern bands, Phys. Rev. B **90**, 245106 (2014).

[85] G. Murthy, E. Shimshoni, and H. A. Fertig, Spin-valley coherent phases of the $\nu = 0$ quantum Hall state in bilayer graphene, Phys. Rev. B **96**, 245125 (2017).

[86] F. Paoletti, L. Fanfarillo, M. Capone, and A. Amaricci, Topological gap opening without symmetry breaking from dynamical quantum correlations, Phys. Rev. B **109**, 075148 (2024).

[87] S. Sachdev, *Quantum Phase Transitions*, 2nd ed. (Cambridge University Press, Cambridge, UK, 2011).

[88] S. L. Sondhi, S. M. Girvin, J. P. Carini, and D. Shahar, Continuous quantum phase transitions, Rev. Mod. Phys. **69**, 315 (1997).

[89] G. Jotzu, M. Messer, R. Desbuquois, M. Lebrat, T. Uehlinger, D. Greif, and T. Esslinger, Experimental realization of the topological Haldane model with ultracold fermions, Nature (London) **515**, 237 (2014).

[90] T.-L. Dao, M. Ferrero, P. S. Cornaglia, and M. Capone, Mott transition of fermionic mixtures with mass imbalance in optical lattices, Phys. Rev. A **85**, 013606 (2012).

[91] M. Gröbner, P. Weinmann, E. Kirilov, H.-C. Nägerl, P. S. Julienne, C. R. Le Sueur, and J. M. Hutson, Observation of interspecies Feshbach resonances in an ultracold ^{39}K - ^{133}Cs mixture and refinement of interaction potentials, Phys. Rev. A **95**, 022715 (2017).

[92] P. Ajayan, P. Kim, and K. Banerjee, Two-dimensional van der Waals materials, Phys. Today **69** (9), 38 (2016).

[93] A. F. Young and L. S. Levitov, Capacitance of graphene bilayer as a probe of layer-specific properties, Phys. Rev. B **84**, 085441 (2011).

[94] B. M. Hunt, J. I. A. Li, A. A. Zibrov, L. Wang, T. Taniguchi, K. Watanabe, J. Hone, C. R. Dean, M. Zaletel, R. C. Ashoori, and A. F. Young, Direct measurement of discrete valley and orbital quantum numbers in bilayer graphene, Nat. Commun. **8**, 948 (2017).

[95] K. Moon, H. Mori, K. Yang, S. M. Girvin, A. H. MacDonald, L. Zheng, D. Yoshioka, and S.-C. Zhang, Spontaneous interlayer coherence in double-layer quantum Hall systems: Charged vortices and Kosterlitz-Thouless phase transitions, Phys. Rev. B **51**, 5138 (1995).

[96] J. Eisenstein, Evidence for spontaneous interlayer phase coherence in a bilayer quantum Hall exciton condensate, Solid State Commun. **127**, 123 (2003).

[97] R. M. Lutchyn, E. Rossi, and S. Das Sarma, Spontaneous interlayer superfluidity in bilayer systems of cold polar molecules, Phys. Rev. A **82**, 061604(R) (2010).

[98] J. Li, H. Fu, Z. Yin, K. Watanabe, T. Taniguchi, and J. Zhu, Metallic phase and temperature dependence of the $\nu = 0$ quantum Hall state in bilayer graphene, Phys. Rev. Lett. **122**, 097701 (2019).